



Figures and figure supplements

Coupling between the DEAD-box RNA helicases Ded1p and eIF4A

Zhaofeng Gao et al

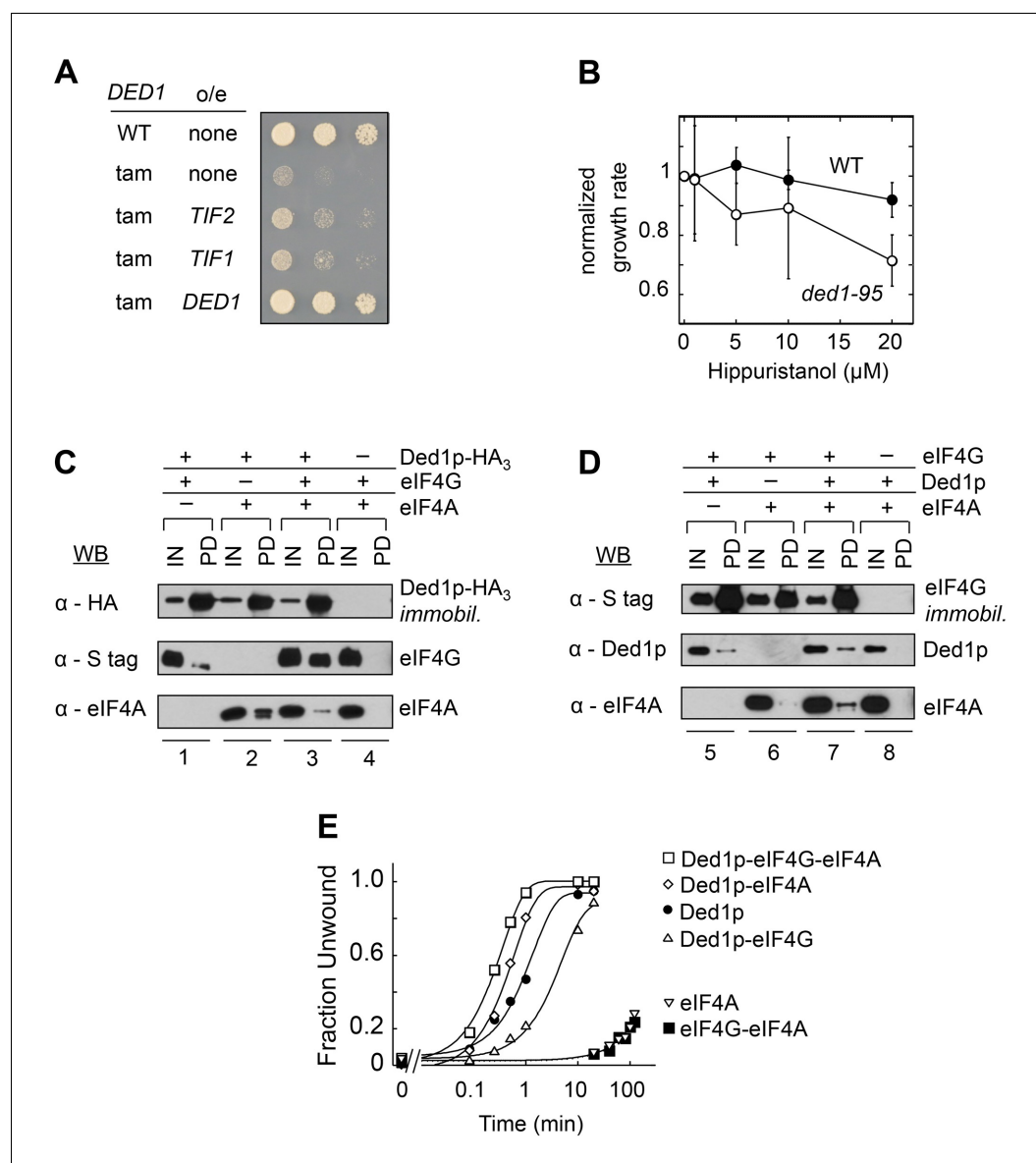


Figure 1. Direct interactions between Ded1p, eIF4A and eIF4G. (A) Effect of *EIF4A* (*TIF1*, *TIF2*) overexpression (o/e) on growth of the *DED1*-tam allele. Yeast with either wild type *DED1* (WT), or *DED1*-tam (tam) as a sole copy of *DED1* were transformed with a high copy plasmid containing either no insert (none) or *TIF1*, *TIF2*, or *DED1*. Serial dilutions of each strain were spotted at identical concentrations on selective media and grown at 16°C. (B) Impact of increasing concentrations of the eIF4A inhibitor hippuristanol on the growth of yeast with either wild type *DED1* (WT), or the temperature sensitive *ded1-95* (*Ded1p*^{T408I}, Figure 1—figure supplement 1) allele as the sole copy. Growth rates were measured at 37°C and normalized to the growth rate without inhibitor. Error bars represent one standard deviation of three independent measurements. (C) Pull-down of purified eIF4A, eIF4G, or both, with immobilized HA-tagged Ded1p. Reactions were performed in the presence of RNases. eIF4G contained an S-tag. Input (IN) lanes show 3% of total reaction volume. Pull-down (PD) lanes show entire sample. Relative band intensities (pull-down compared to input): reaction 1, Ded1p: 460% \pm 18%, eIF4G: 31% \pm 12%; reaction 2: Ded1p: 413% \pm 58%, eIF4A: 96% \pm 55%; reaction 3, Ded1p: 592% \pm 113%, eIF4G: 74% \pm 9%, eIF4A: 25% \pm 21%. Errors represent one standard deviation of multiple independent experiments. (D) Pull-down of purified eIF4A, Ded1p, or both, with immobilized, S-tagged eIF4G. Reactions were performed in the presence of RNases. Input (IN) lanes show 3% of total reaction volume. Pull-down (PD) lanes show entire sample. Relative band intensities (pull-down compared to input): reaction 5, eIF4G: 440% \pm 113%, Ded1p: 14% \pm 7%; reaction 6: eIF4G: 280% \pm 29%, eIF4A: 3% \pm 2%; reaction 7, eIF4G: 473% \pm 27%, Ded1p: 33% \pm 11%, eIF4A: 15% \pm 5%. Errors represent one standard deviation of multiple independent experiments. (E) Unwinding activity of Ded1p, eIF4A, with and without eIF4G, Figure 1 continued on next page

Figure 1 continued

and in combination. Representative unwinding reaction with 0.5 nM RNA duplex (16 bp, 25 nt 3'-overhang, for sequences see **Supplementary file 1A**), 0.1 μ M Ded1p, 0.1 μ M eIF4G, 2 μ M eIF4A, 4 mM ATP (0.2% v/v DMSO). Lines represent the best fit to the integrated first order rate law. See also **Figure 1—figure supplement 1** and **Supplementary file 1A**.

DOI: [10.7554/eLife.16408.002](https://doi.org/10.7554/eLife.16408.002)

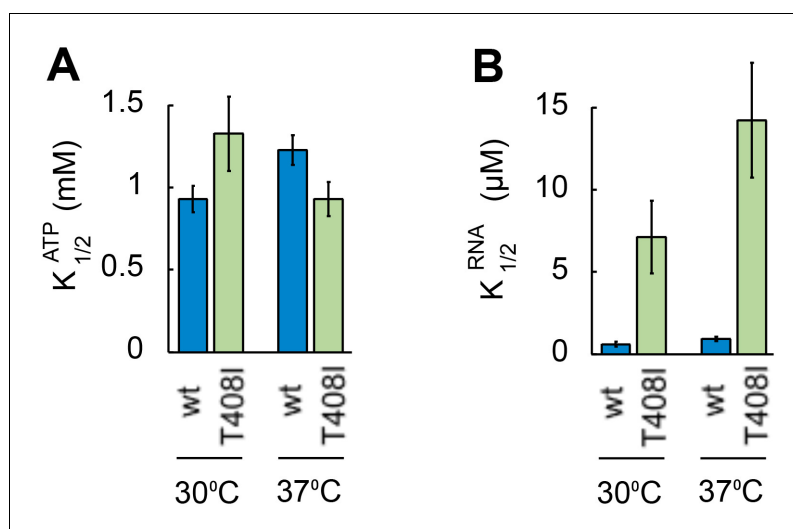


Figure 1—figure supplement 1. Ded1p^{T408I} is deficient in RNA binding. (A) ATP affinity of Ded1p^{T408I} and WT Ded1p. Apparent ATP affinities ($K_{1/2}^{ATP}$) of WT Ded1p and Ded1p^{T408I} for ATP at 30°C and 37°C were measured through RNA-stimulated ATPase activity of the proteins with the substrate containing a 16 bp duplex and 25 nt unpaired 3' overhang (Putnam and Jankowsky, 2013). Values for $K_{1/2}^{ATP}$ were calculated by fitting ATP titrations to the MichaelisMenten model (Putnam and Jankowsky, 2013). k_{cat} for ATP did not notably differ between Ded1p^{T408I} and WT Ded1p (data not shown). (B) RNA affinity for Ded1p^{T408I} and WT Ded1p. Apparent RNA affinities ($K_{1/2}^{RNA}$) of WT Ded1p and Ded1p^{T408I} for RNA at 30°C and 37°C were measured through RNA-stimulated ATPase activity of the proteins as in panel A. Values for $K_{1/2}^{RNA}$ were calculated by fitting RNA titrations to the Michaelis Menten model (Putnam and Jankowsky, 2013). The data indicate an RNA binding defect in Ded1p^{T408I}.

DOI: 10.7554/eLife.16408.003

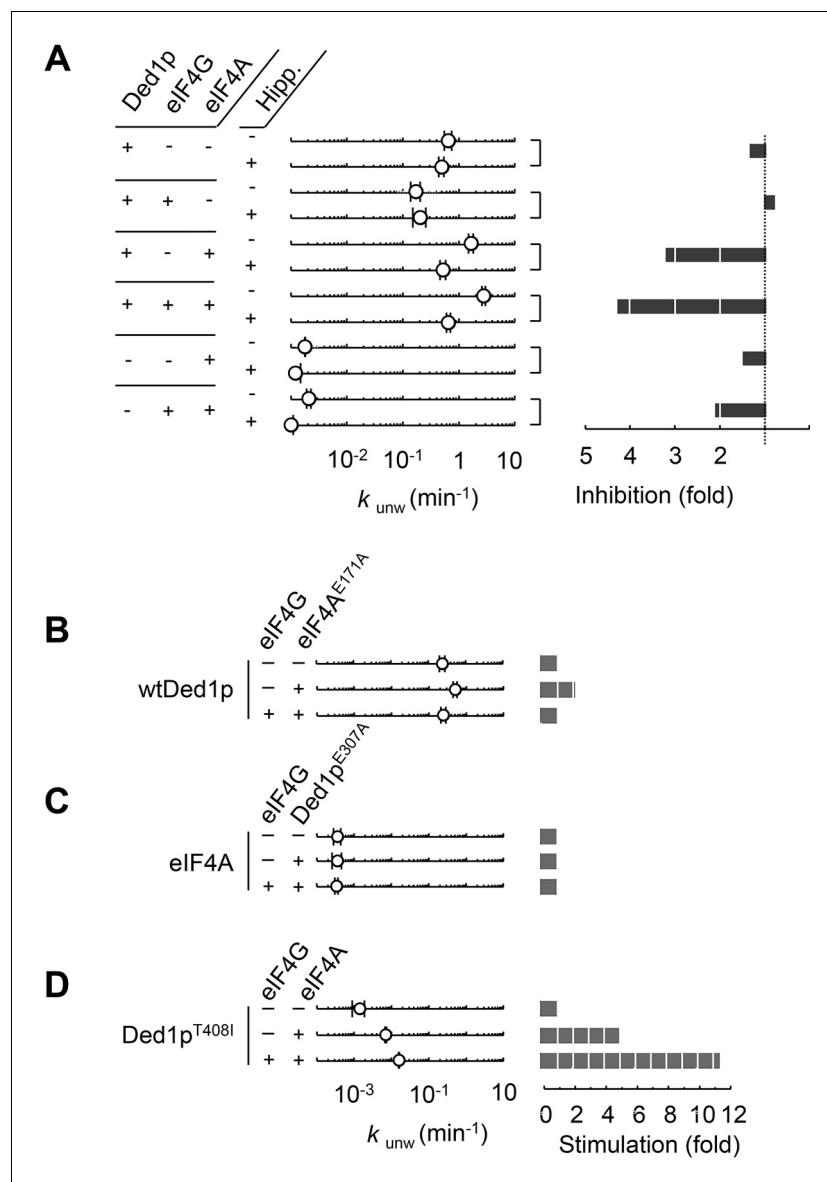


Figure 2. Ded1p is the unwinding module in complexes with eIF4A and eIF4G. (A) Impact of hippuristanol on of Ded1p, eIF4A, with and without eIF4G, and in combination. Reactions were performed as in **Figure 1E** with 0.2% (v/v) DMSO and 20 μ M Hippuristanol, as indicated. *Left panel:* Observed unwinding rate constants (k_{unw}). For representative unwinding reactions see **Figure 2—figure supplement 1**. Error bars represent one standard deviation of at least three independent measurements. *Right panel:* decrease or increase of k_{unw} by hippuristanol. (B) Impact of eIF4A^{E171A} (100 nM) on the unwinding activity of Ded1p (100 nM) with or without eIF4G (100 nM), measured as in **Figure 1E**, but without DMSO. *Left panel:* Observed unwinding rate constants (k_{unw}). Error bars represent one standard deviation of at least three independent measurements. *Right panel:* increase of k_{unw} , compared to reaction without eIF4A^{E171A}. (C) Impact of Ded1p^{E307A} on the unwinding activity of eIF4A with or without eIF4G, measured as in **Figure 2B**. *Left panel:* Observed unwinding rate constants (k_{unw}). Error bars represent one standard deviation of at least three independent measurements. *Right panel:* increase of k_{unw} , compared to reaction without Ded1p^{E307A}. (D) Impact of eIF4A on of Ded1p^{T408I} with or without eIF4G, measured as in **Figure 2B**. *Left panel:* Observed unwinding rate constants (k_{unw}). Error bars represent one standard deviation of at least three independent measurements. *Right panel:* increase of k_{unw} , compared to reaction without eIF4A. See also **Figure 2—figure supplement 1**.

DOI: 10.7554/eLife.16408.004

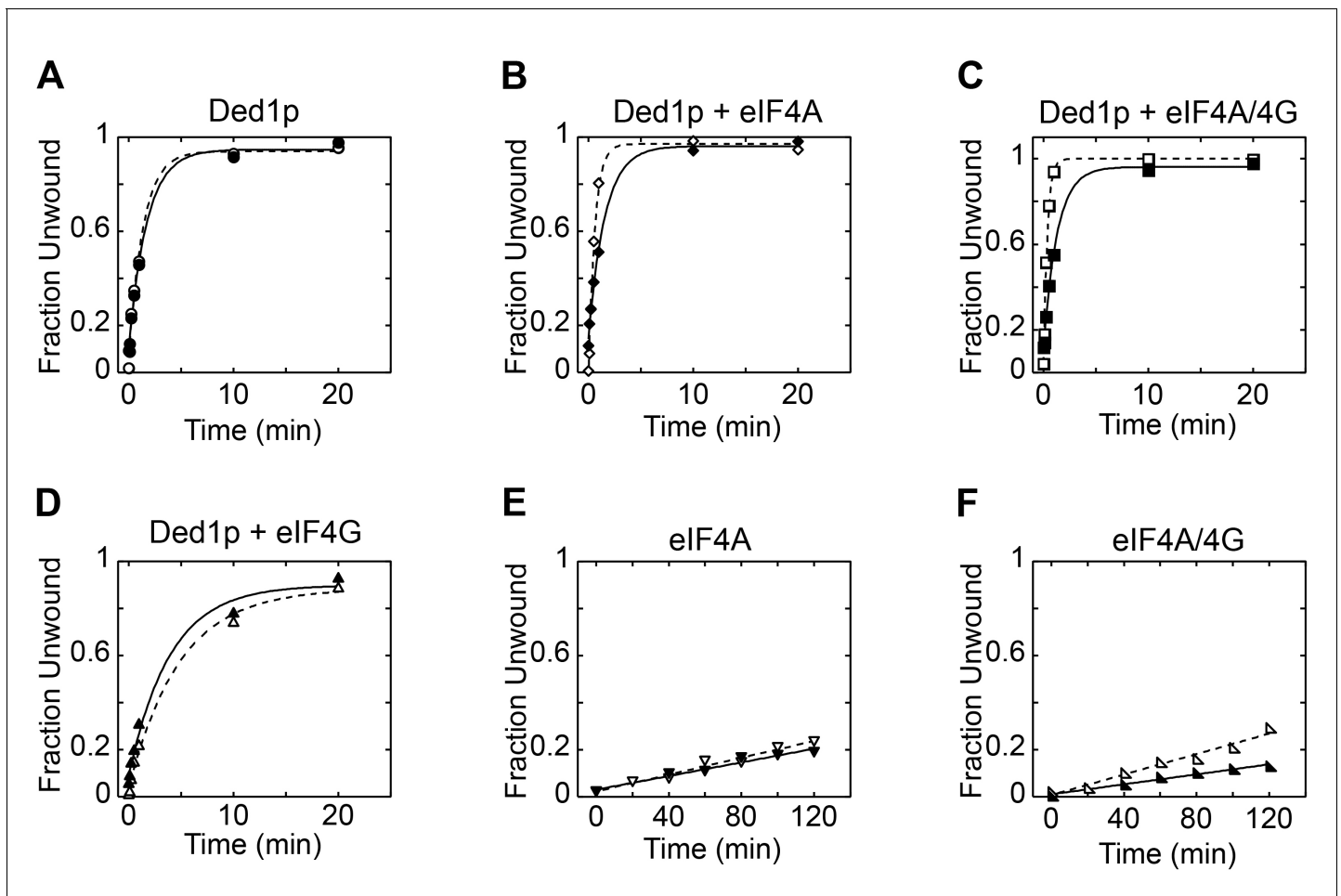


Figure 2—figure supplement 1. Reaction progress curves for **Figure 2A**. Representative unwinding reactions for **Figure 2A**, with (A) Ded1p, (B) Ded1p and eIF4A, (C) Ded1p, eIF4A, and eIF4G, (D) Ded1p and eIF4G, (E) eIF4A, (F) eIF4A and eIF4G. In each panel, open shapes represent reactions without hippuristanol; filled shapes represent reactions with hippuristanol. Lines represent the best fit to the integrated first order rate law.

DOI: [10.7554/eLife.16408.005](https://doi.org/10.7554/eLife.16408.005)

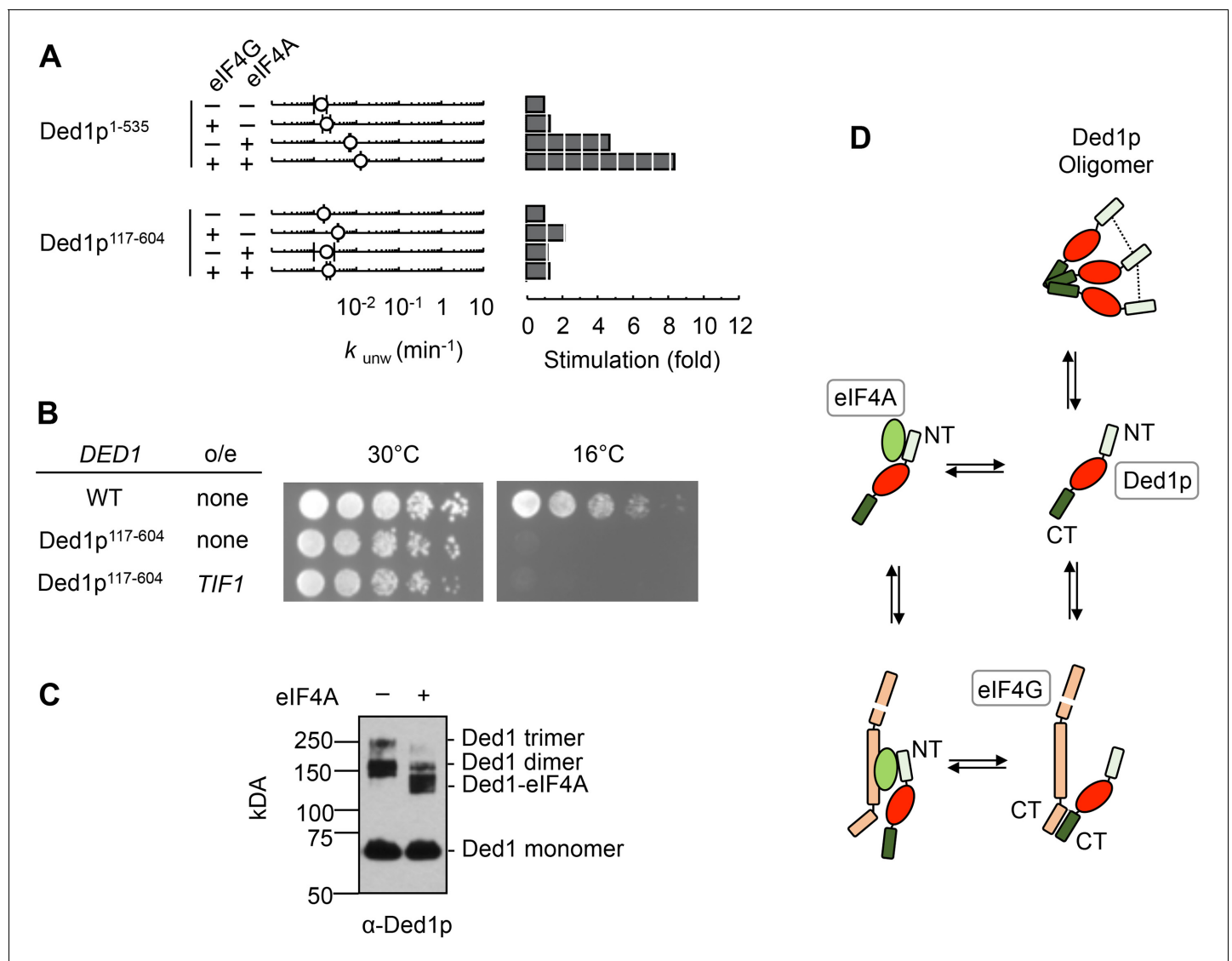


Figure 3. The N-terminus of Ded1p is critical for the interaction with eIF4A. (A) Impact of eIF4A on of Ded1p¹⁻⁵³⁵ (C-terminus deleted, upper panels) and Ded1p¹¹⁷⁻⁶⁰⁴ (N-terminus deleted, lower panels) with or without eIF4G, measured as in **Figure 2B**. *Left panel*: Observed unwinding rate constants (k_{unw}). Error bars represent one standard deviation of at least three independent measurements. *Right panel*: increase of k_{unw} , compared to reactions with Ded1p alone. (B) Effect of the deletion of the N-terminus of Ded1p (Ded1p¹¹⁷⁻⁶⁰⁴), without or with EIF4A (*TIF1*) overexpression (o/e), on growth in yeast at 30°C and 16°C. (C) Formaldehyde crosslinking of Ded1p without and with eIF4A in the presence of RNA (16 bp, 25 nt 3'-overhang) and ADPNP. Mobilities of the Ded1p trimer, dimer, monomer, and the Ded1p-eIF4A complex are indicated. Proteins were visualized by western blot (α -Ded1p). (D) Schematic model for the basic functional architecture of Ded1p-eIF4A and Ded1p-eIF4A-eIF4G complexes. Ovals represent the helicase cores of Ded1p (red) and eIF4A (green). C- and N-termini of Ded1p and eIF4G are marked. The dotted lines between the N-termini in the Ded1p trimer indicate interactions between the N-termini that contribute to oligomerization. See also **Figure 3—figure supplement 1** and **Supplementary file 1A**. DOI: 10.7554/eLife.16408.006

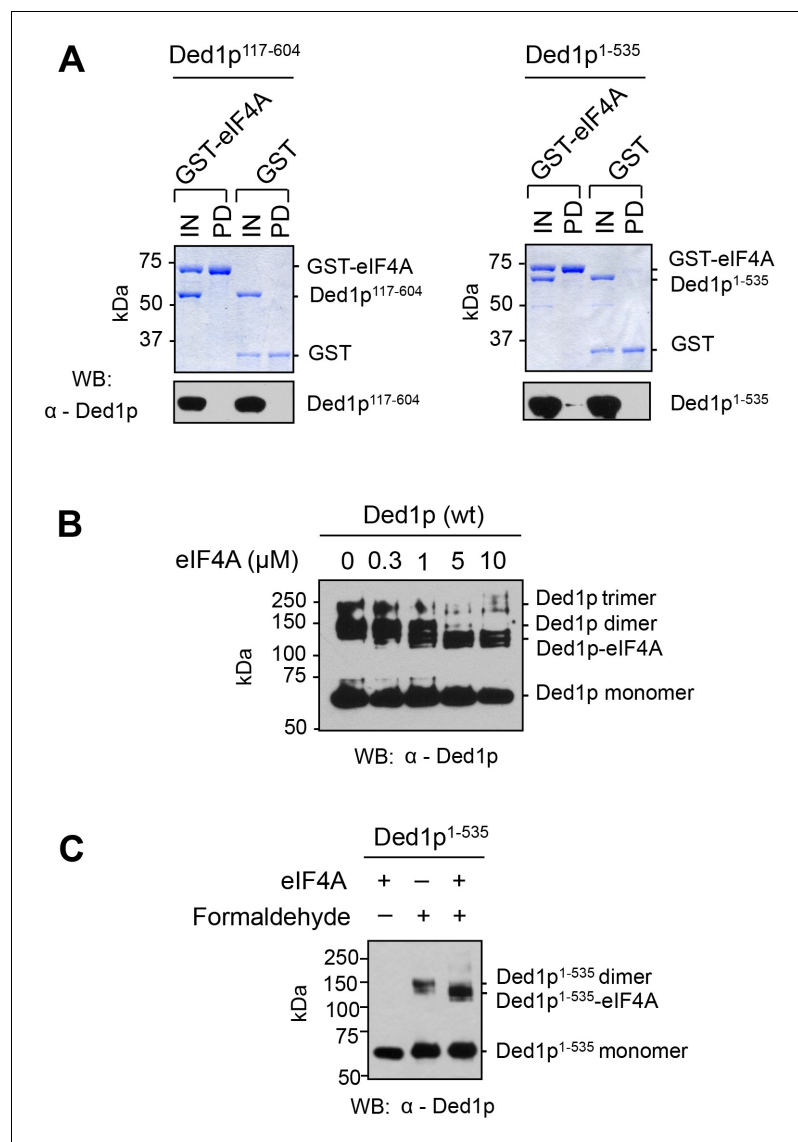


Figure 3—figure supplement 1. Direct interaction between eIF4A and the amino terminus of Ded1p. (A) Pull-down of purified Ded1p¹¹⁷⁻⁶⁰⁴ or Ded1p¹⁻⁵³⁵, with immobilized GST-eIF4A. (1500 nM GST-eIF4A or GST, 1500 nM Ded1p¹¹⁷⁻⁶⁰⁴ or Ded1p¹⁻⁵³⁵, and 20 μg/mL RNases A at 8°C). Ded1p was probed with the α-Ded1p antibody. Deletion of the N-terminus eliminates the interaction between Ded1p and eIF4A. Input (IN) lanes show 10% of total reaction volume. Pull-down (PD) lanes show entire sample. The relative band intensities (pull-down compared to input) for the reaction with GST-eIF4A and Ded1p¹⁻⁵³⁵: GST-eIF4A: 160% ± 17%, Ded1p¹⁻⁵³⁵: 3% ± 1%. Errors represent one standard deviation of multiple independent experiments. No signal for Ded1p¹¹⁷⁻⁶⁰⁴ was detected in the pull-down. (B) Formaldehyde crosslinking of Ded1p, with increasing concentrations of eIF4A, in the presence of RNA (16 bp, 25 nt 3'-overhang) and ADPNP. Mobilities of the Ded1p trimer, dimer, monomer, and the Ded1p-eIF4A complex are indicated. Proteins were visualized by western blot (α-Ded1p). Increasing concentrations of eIF4A diminish the Ded1p trimer and dimer species. (C) Formaldehyde crosslinking of Ded1p¹⁻⁵³⁵ without and with eIF4A in the presence of RNA (16bp, 25 nt 3'-overhang) and ADPNP. This experiment was performed to directly verify the weak interaction between Ded1p and eIF4A detected by pull-down in panel (A). Deletion of C-terminus of Ded1p diminishes formation of the Ded1p trimer (Putnam et al., 2015). Mobilities of the Ded1p dimer, monomer, and the Ded1p-eIF4A complex are indicated. Ded1p was visualized by western blot (α-Ded1p).

DOI: [10.7554/eLife.16408.007](https://doi.org/10.7554/eLife.16408.007)

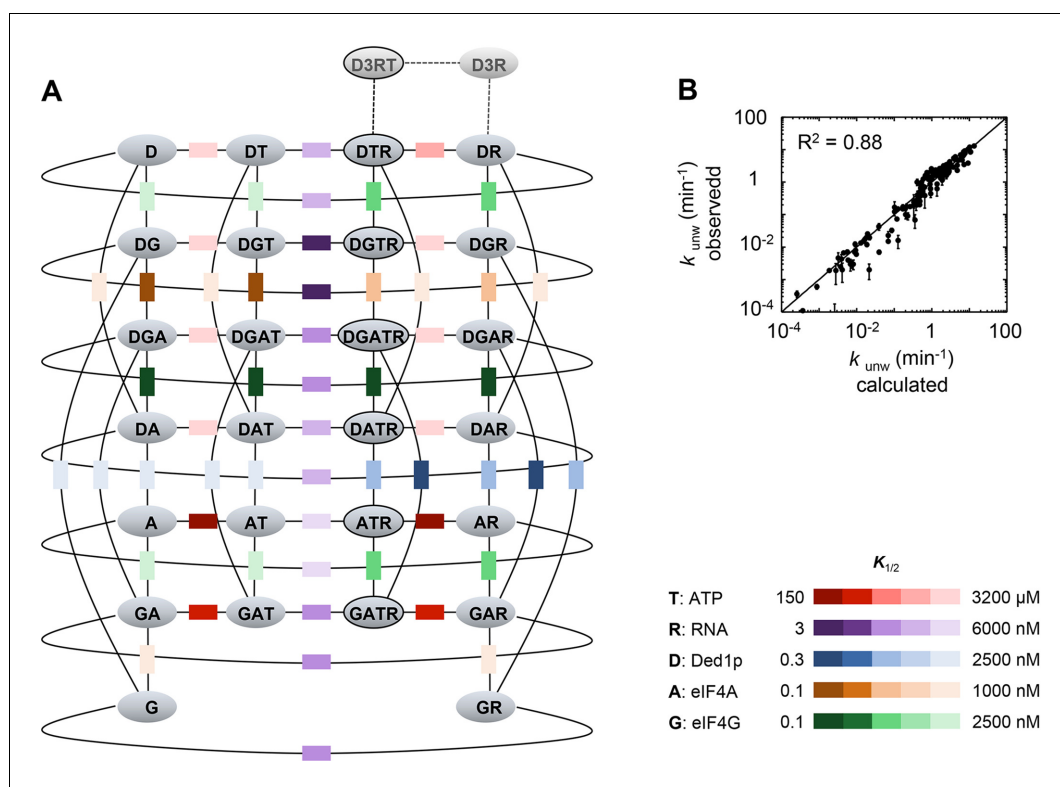


Figure 4. Thermodynamic framework for the interactions between Ded1p, eIF4A and eIF4G. (A) Graphic representation of the framework. Ovals represent the complexes containing Ded1p (D), eIF4A (A), eIF4G (G), RNA (R), ATP (T). D3 indicates the Ded1p timer (Putnam et al., 2015). Black lines mark a transition from one complex to another through binding of one of the components. Colored squares indicate the calculated equilibrium dissociation constant ($K_{1/2}$) for the transition, as shown in the legend at the lower right. For visual reasons, the framework does not depict specific states for ATP-bound eIF4A. Equilibrium constants for all individual transitions are listed in **Supplementary file 2**. (B) Observed apparent unwinding rate constants versus those calculated with the model in panel (A). Measured and calculated rate constants from different reaction conditions are listed without reference to the specific reaction conditions, solely to visualize the overall agreement between observed and calculated values. For fitting parameters see **Figure 4—figure supplement 5** and **Supplementary file 2**. The black line represents a diagonal, R^2 is the correlation coefficient for a linear fit of the shown data to this line. Error bars mark the standard deviation for the observed values. See also **Figure 4—figure supplements 1–6** and **Supplementary files 2,3**.

DOI: [10.7554/eLife.16408.008](https://doi.org/10.7554/eLife.16408.008)

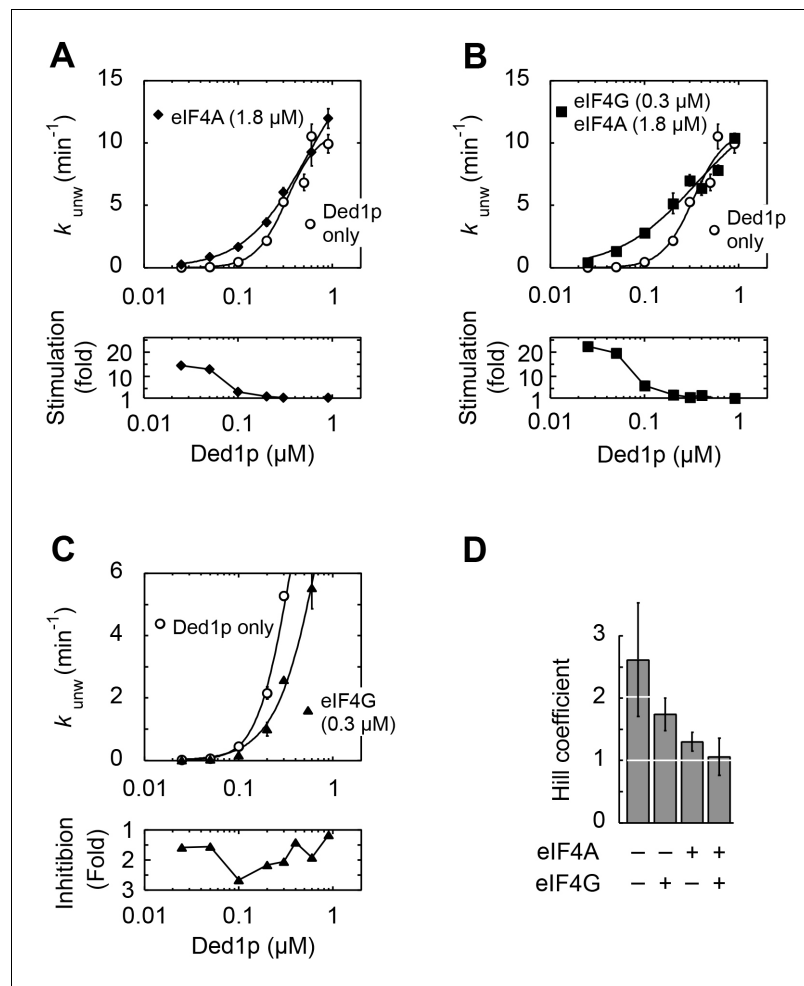


Figure 4—figure supplement 1. Impact of the Ded1p concentration on the modulation of its unwinding activity by eIF4A and eIF4G. All unwinding reactions were performed as in **Figure 2B** at the indicated Ded1p, eIF4A and eIF4G, and ATP concentrations. Apparent rate constants (k_{unw}) represent the mean of at least three independent measurements. Error bars indicate one standard deviation. (A–C) *Upper panels:* Impact of eIF4A (A), eIF4A and eIF4G (B) and eIF4G alone (C) at increasing Ded1p concentration at 4 mM ATP. Lines represent the best fit to a binding isotherm. Note the different scale of the y-axis in (C). *Lower panels:* Fold increase or decrease of k_{unw} at each Ded1p concentration over the reaction with Ded1p alone. (D) Hill coefficients calculated from Ded1p binding isotherms (A–C) in the presence of the indicated combinations of eIF4G and eIF4A.

DOI: [10.7554/eLife.16408.009](https://doi.org/10.7554/eLife.16408.009)

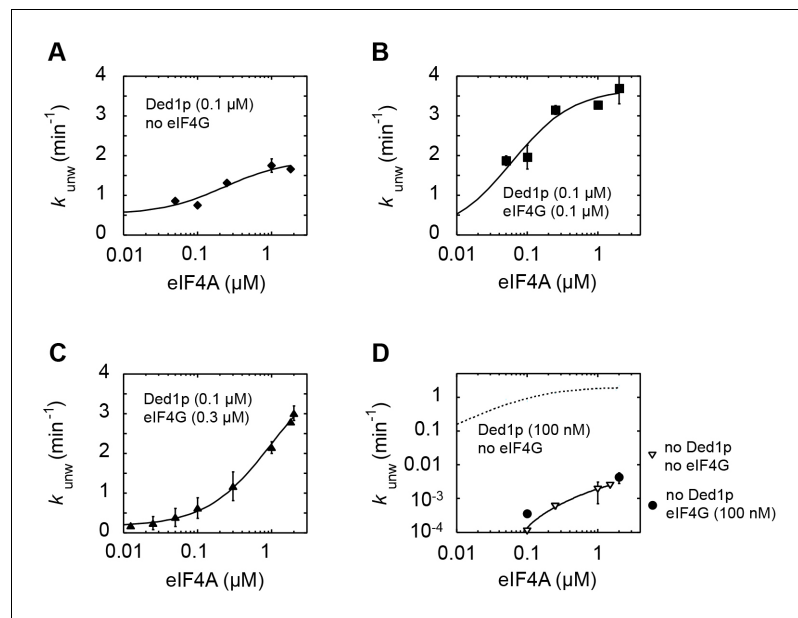


Figure 4—figure supplement 2. Impact of eIF4A concentration on the modulation of Ded1p unwinding activity by eIF4A and eIF4G. All unwinding reactions were performed as in **Figure 2B** at the indicated Ded1p, eIF4A and eIF4G, and ATP concentrations. Apparent rate constants (k_{unw}) represent the mean of at least three independent measurements. Error bars indicate one standard deviation. (A–C) Impact of increasing concentrations of eIF4A at a fixed Ded1p concentration (A), and fixed Ded1p and two different eIF4G concentrations (B,C) at 4 mM ATP. Lines represent the best fit to a binding isotherm. (D) Impact of increasing concentrations of eIF4A on unwinding in the absence and presence of eIF4G, without Ded1p. The corresponding curve in the presence of only Ded1p is shown as dotted line for reference.

DOI: [10.7554/eLife.16408.010](https://doi.org/10.7554/eLife.16408.010)

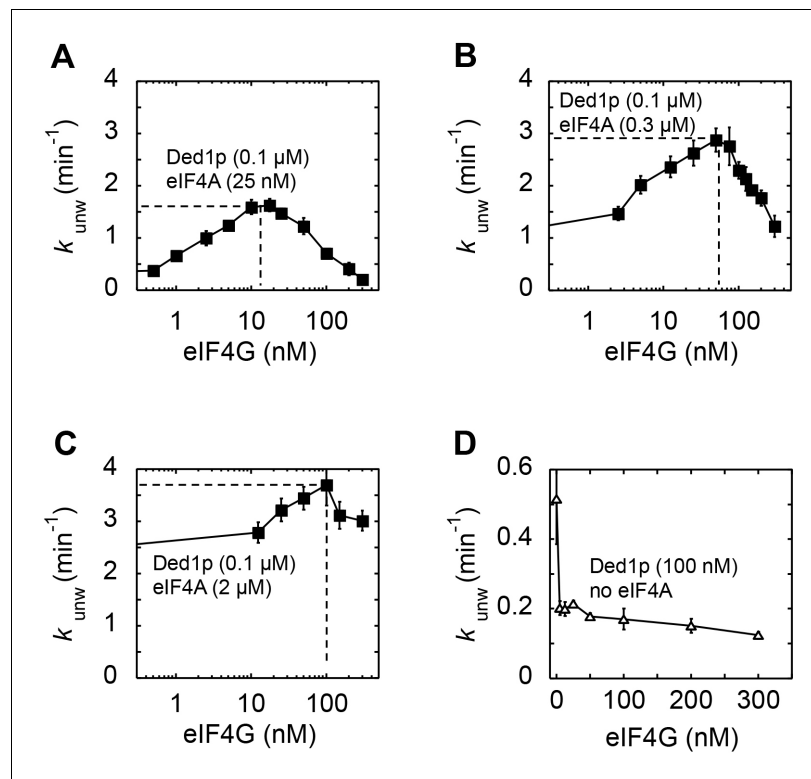


Figure 4—figure supplement 3. Impact of eIF4G concentration on the modulation of Ded1p unwinding activity by eIF4A and eIF4G. All unwinding reactions were performed as in **Figure 2B** at the indicated Ded1p, eIF4A and eIF4G, and ATP concentrations. Apparent rate constants (k_{unw}) represent the mean of at least three independent measurements. Error bars indicate one standard deviation. (A–C) Impact of increasing concentrations of eIF4G at a fixed Ded1p concentration at 4 mM ATP, and increasing concentrations of eIF4A, as indicated. Lines represent a trend, dashed lines mark the maximal observed unwinding rate constant. (D) Impact of increasing concentrations of eIF4G on Ded1p (100 nM, no eIF4A) activity in the presence of 4 mM ATP. Note the scale of y and x-axis.

DOI: [10.7554/eLife.16408.011](https://doi.org/10.7554/eLife.16408.011)

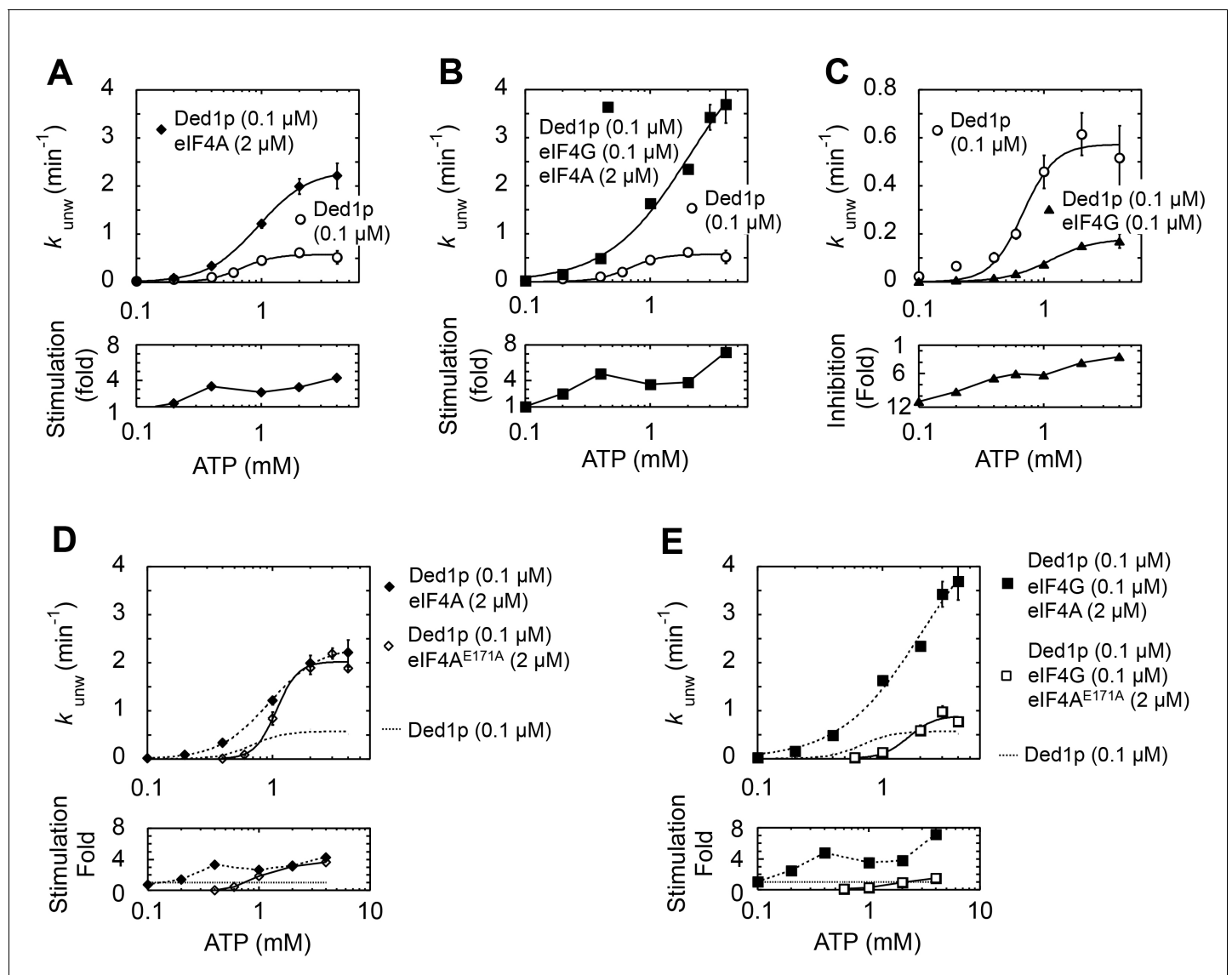


Figure 4—figure supplement 4. Impact of ATP concentration on the modulation of Ded1p unwinding activity by eIF4A and eIF4G. All unwinding reactions were performed as in **Figure 2B** at the indicated Ded1p, eIF4A and eIF4G, and ATP concentrations. Apparent rate constants (k_{unw}) represent the mean of at least three independent measurements. Error bars indicate one standard deviation. (A–C) *Upper panels*: Impact of ATP on reactions with fixed concentrations of Ded1p and eIF4A (A), Ded1p, eIF4A, and eIF4G (B), and Ded1p and eIF4G (C). Lines represent the best fit to a binding isotherm. Note the different scale of the y-axis in (C). *Lower panels*: Fold increase or decrease of k_{unw} by eIF4A, eIF4G, or both, over the reaction with Ded1p alone. (D) *Upper panels*: Impact of ATP on the unwinding reaction with Ded1p and the ATP-binding deficient eIF4A^{E171A} (black solid line, open diamonds). The reactions with Ded1p and WT eIF4A (dotted line, filled diamonds) (A) and with Ded1p alone (dotted line, no symbols) (A) are shown as reference. *Lower panels*: Fold increase or decrease of k_{unw} by WT eIF4A, or eIF4A^{E171A}, over the reaction with Ded1p alone. (E) *Upper panels*: Impact of ATP on the unwinding reaction with Ded1p, eIF4G and the ATP-binding deficient eIF4A^{E171A} (black line, open squares). The reactions with Ded1p, eIF4G and WT eIF4A (dotted line, filled squares) (B) and with Ded1p alone (dotted line, no symbols) (B) are shown as reference. *Lower panels*: Fold increase or decrease of k_{unw} by eIF4G with WT eIF4A or eIF4A^{E171A}, over the reaction with Ded1p alone. (E) *Upper panels*: Impact of ATP on the unwinding reaction with Ded1p, eIF4G and the ATP-binding deficient eIF4A^{E171A} (black line, open squares). The reactions with Ded1p, eIF4G and WT eIF4A (dotted line, filled squares) (B) and with Ded1p alone (dotted line, no symbols) (B) are shown as reference. *Lower panels*: Fold increase or decrease of k_{unw} by eIF4G with WT eIF4A or eIF4A^{E171A}, over the reaction with Ded1p alone.

DOI: 10.7554/eLife.16408.012

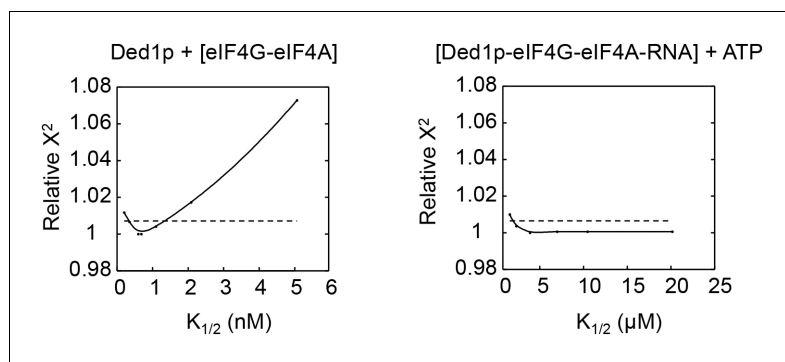


Figure 4—figure supplement 5. Relative Chi square values (X^2) for variations of two representative parameters. Left panel: Ded1p binding to pre-formed eIF4A-eIF4G complex; right panel: ATP binding to Ded1p-eIF4G-eIF4A-RNA complex). The two examples were chosen to illustrate a case where both, increase and decrease in the parameter ($K_{1/2}$) relative to the optimal value results in a poorer fit (left panel), and for a case where only a decrease of the parameter, but not an increase result in a poorer fit (right fit). Cases for the latter scenario are restricted to ATP binding and marked in the **Supplementary file 2** with an '>' sign. Relative X^2 represent the X^2 obtained for the entire thermodynamic model for the parameter on the X axis divided by the smallest (optimal) X^2 . For the optimal parameter, the relative $X^2 = 1$. Dotted lines mark the 95% confidence interval. This interval is given for each parameter in the **Supplementary file 2**. Values for X^2 represent the quality of the fit for the varied parameter to the entire thermodynamic model (**Figure 4A**).

DOI: [10.7554/eLife.16408.013](https://doi.org/10.7554/eLife.16408.013)

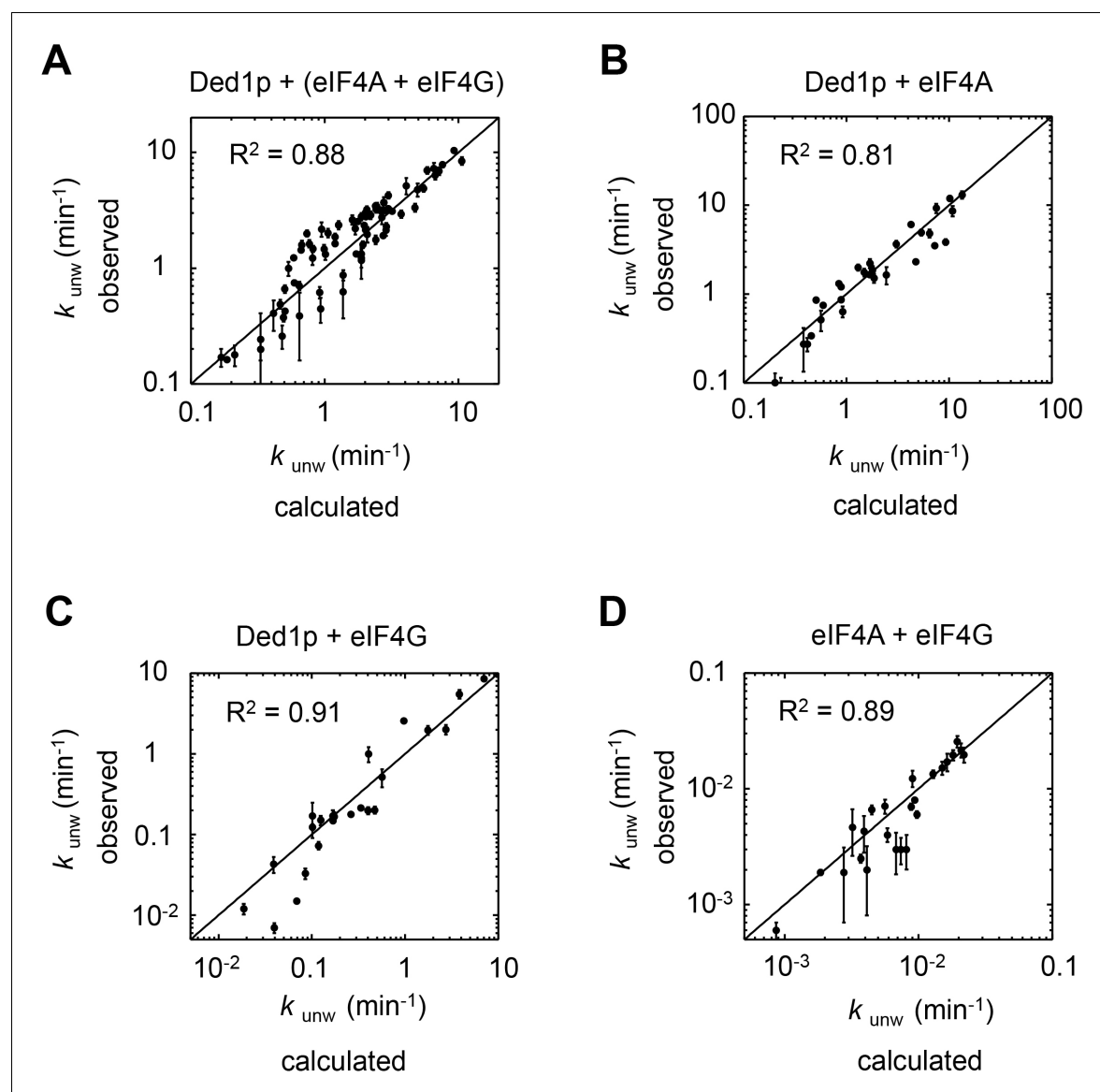


Figure 4—figure supplement 6. The thermodynamic model adequately describes observed data for each subset of complexes. The correlation between observed and calculated unwinding rate constants (k_{unw}) for subsets of the complexes, as indicated. R^2 is the correlation coefficient of a linear fit of the data in each panel to a diagonal (black line). Error bars mark the 95% confidence interval for the calculated data. For fitting parameters see [Supplementary file 2](#).

DOI: [10.7554/eLife.16408.014](https://doi.org/10.7554/eLife.16408.014)

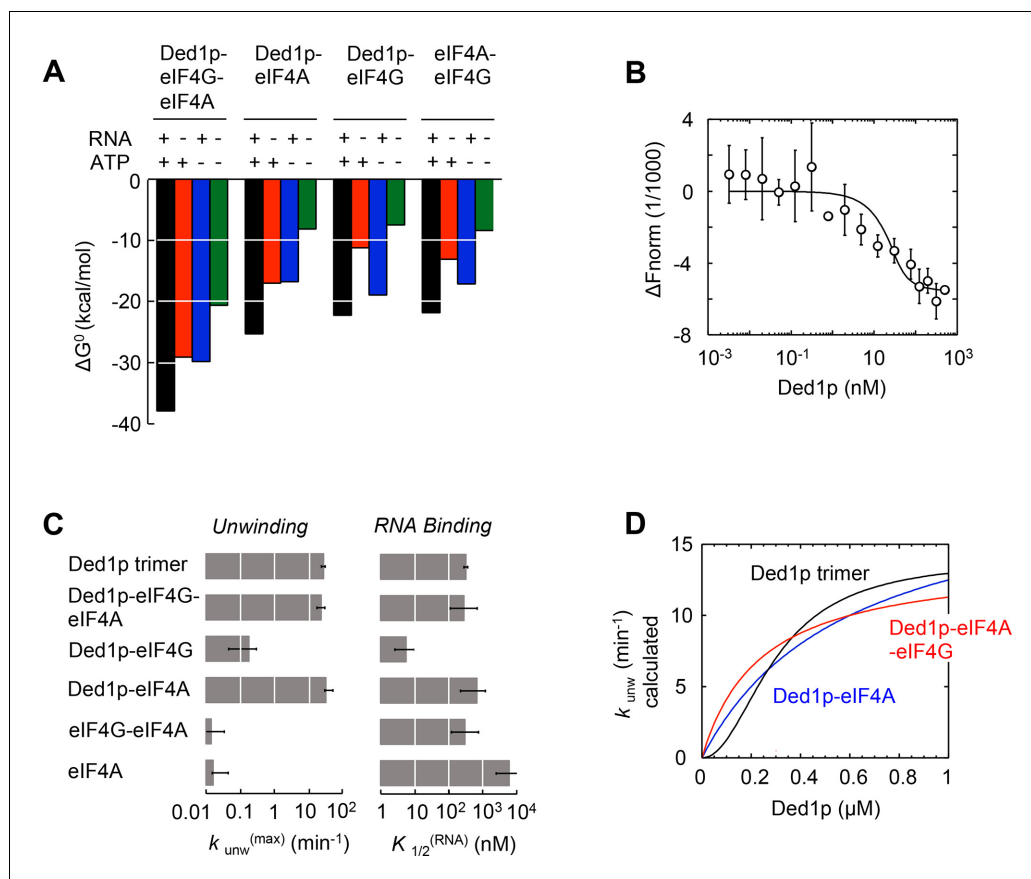


Figure 5. Functional parameters of complexes with Ded1p, eIF4A, or both. (A) Free energies ΔG° for complexes formed between Ded1p, eIF4A, eIF4G, RNA (25 nt 3'-overhang, 16 bp duplex) and ATP in the combinations shown, calculated with the model in **Figure 4A**. (B) MST measurement of Ded1p binding to eIF4A-eIF4G (30 nM eIF4G, 36 nM Cy5-labeled eIF4A, increasing concentrations of Ded1p as indicated, 25 μg/mL RNase A, 23°C). Datapoints show the change in fluorescence signal at the indicated Ded1p concentrations, normalized to the signal without Ded1p. Error bars indicate one standard deviation of multiple independent measurements. Datapoints were fitted with the quadratic form of the binding isotherm ($K'_{1/2} < 6.6$ nM). (C) Unwinding rate constants ($k_{\text{unw}}^{(\text{max})}$, ATP and protein saturation, RNA: 25 nt 3' overhang, 16 bp duplex) and RNA affinity ($K_{1/2}^{(\text{RNA})}$, ATP saturation) for complexes formed between Ded1p, eIF4A, eIF4G, and, for comparison, for Ded1p and eIF4A, calculated with the model in **Figure 4A**. (D) Unwinding rate constants (RNA: 25 nt 3' overhang, 16 bp duplex) for the Ded1p trimer, the Ded1p-eIF4A, and the Ded1p-eIF4A-eIF4G complex as function of the Ded1p concentration (ATP saturation, eIF4A = 2000 nM, eIF4G = 100 nM), calculated with the model in **Figure 4A**. See also **Figure 5—figure supplement 1**.

DOI: [10.7554/eLife.16408.015](https://doi.org/10.7554/eLife.16408.015)

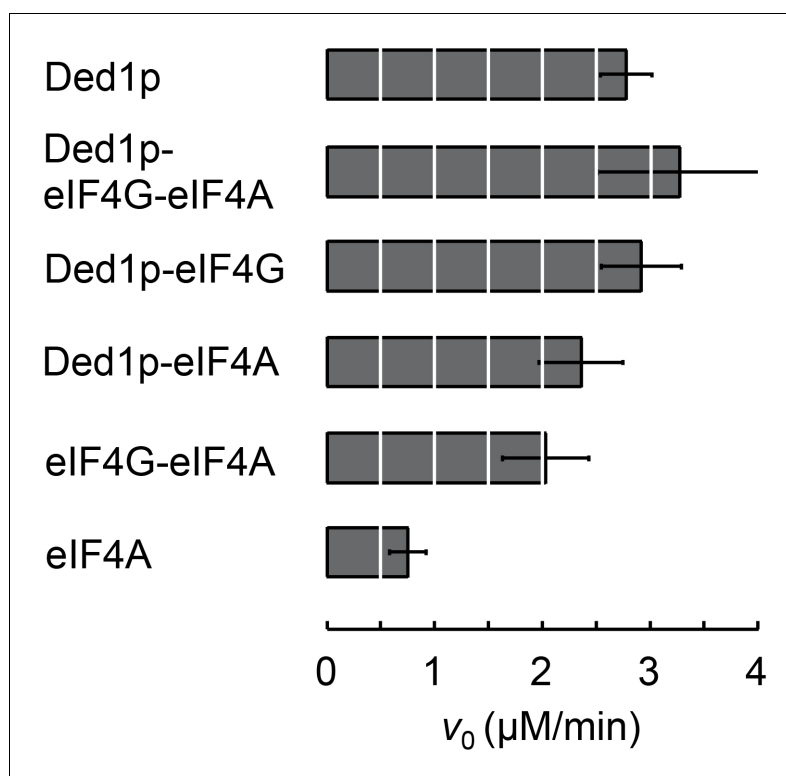


Figure 5—figure supplement 1. ATPase activity of complexes formed between Ded1p, eIF4A, and eIF4G at RNA and ATP saturation. ATPase reactions were performed with Ded1p (100 nM), eIF4A (2000 nM), eIF4G (100 nM), as indicated, and with RNA (16bp, 25nt 3'-overhang, 40 μM) and ATP (4 mM). Initial rates for the ATPase reactions (v_0) under these conditions represent ATP turnover numbers (equivalent to k_{cat}). Values were measured as described (Putnam and Jankowsky, 2013).

DOI: [10.7554/eLife.16408.016](https://doi.org/10.7554/eLife.16408.016)

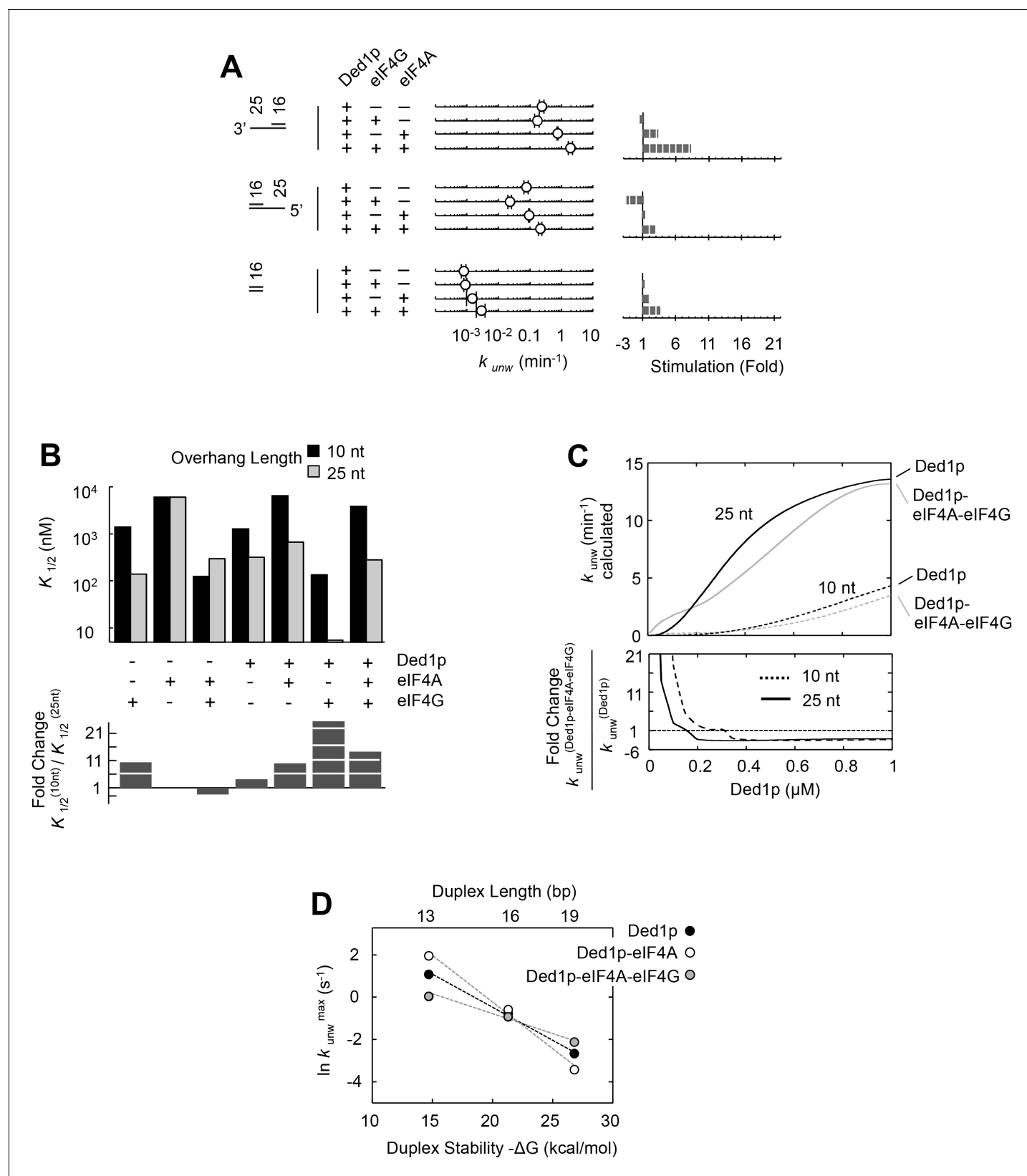


Figure 6. Impact of the substrate architecture on the functional parameters of complexes with Ded1p, eIF4A, and eIF4G. (A) Impact of eIF4A, eIF4G, or both, on the unwinding activity of Ded1p with 5' and 3' tailed substrates (16 bp, 25 nt 3'- or 5'-tail), and blunt-end, shown schematically at the left (numbers indicate nucleotides in unpaired overhang and basepairs in duplex region). Reactions were performed as in **Figure 2B**. Sliding point graphs **Figure 6 continued on next page**

Figure 6 continued

show observed unwinding rate constants (k_{unw} , average of at least three independent measurements), error bars mark one standard deviation. Bar graphs mark increase or decrease of k_{unw} , compared to the reaction with only Ded1p for each substrate. (B) *Upper panel*: Affinities ($K_{1/2}$) for RNA substrates with 10 nt and 25 nt unpaired regions 3' to the duplex (16 bp) for Ded1p, eIF4A, eIF4G alone and in combination as indicated, calculated with the model shown in **Figure 4A**, and with data obtained with two substrates containing either 10 or 25 nt overhangs. For modeling parameters see **Figure 6—figure supplements 2,3, Supplementary file 2** and Materials and methods. *Lower panel*: Fold change in $K_{1/2}$ between the substrates with 10 and 25 nt unpaired regions. (C) *Upper panel*: Apparent unwinding rate constants (k_{unw} , ATP = 4 mM, eIF4A = 100 nM, eIF4G = 100 nM) for Ded1p alone and for the Ded1p-eIF4A-eIF4G complex on RNA substrates with 10 or 25 nt overhangs, 3' to a 16 bp duplex, as function of increasing Ded1p concentration, calculated with the model shown in **Figure 4A**, and with data obtained with two substrates containing either 10 or 25 nt overhangs. *Lower panel*: Fold change in k_{unw} for reactions with Ded1p-eIF4A-eIF4G, compared to reactions with Ded1p alone for both substrates. (D) Unwinding rate constants at ATP and protein saturation for RNA substrates with 25 nt 3' overhangs and 13, 16, and 19 bp duplexes, for Ded1p, the Ded1p-eIF4A complex and the Ded1p-eIF4A-eIF4G complex, calculated with the model shown in **Figure 4**. For modeling parameters see **Figure 4—figure supplements 5,6; Figure 6—figure supplement 2, Supplementary files 2,3** and Materials and methods. See also **Figure 6—figure supplements 1,3**. DOI: 10.7554/eLife.16408.017

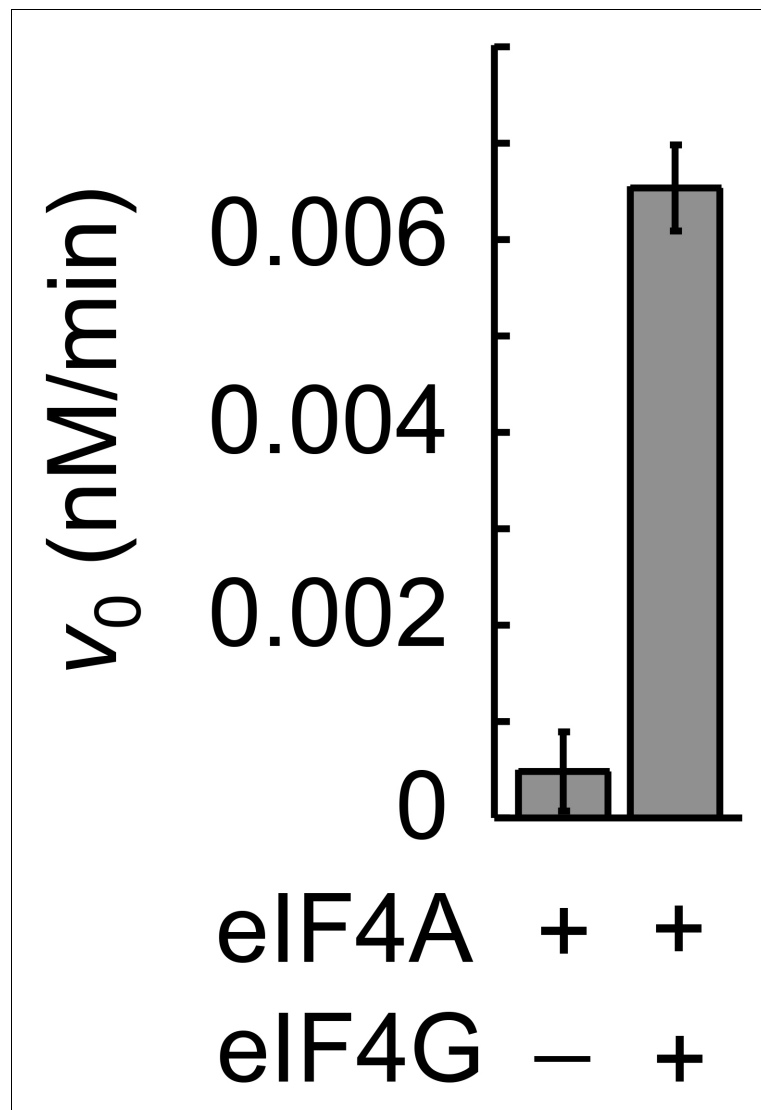


Figure 6—figure supplement 1. Stimulation of unwinding activity of eIF4A by eIF4G with an RNA with a 5' tail. Unwinding reactions were performed in buffer used for all other unwinding reactions at 26°C with 100 nM eIF4A, 300 nM eIF4G, 3 mM ATP, 10 nM RNA (13 bp, 25 nt overhang, 5' to duplex) and 3 μ M unlabeled top strand (13 nt), made from DNA. For sequences see **Supplementary file 1A**.
DOI: [10.7554/eLife.16408.018](https://doi.org/10.7554/eLife.16408.018)

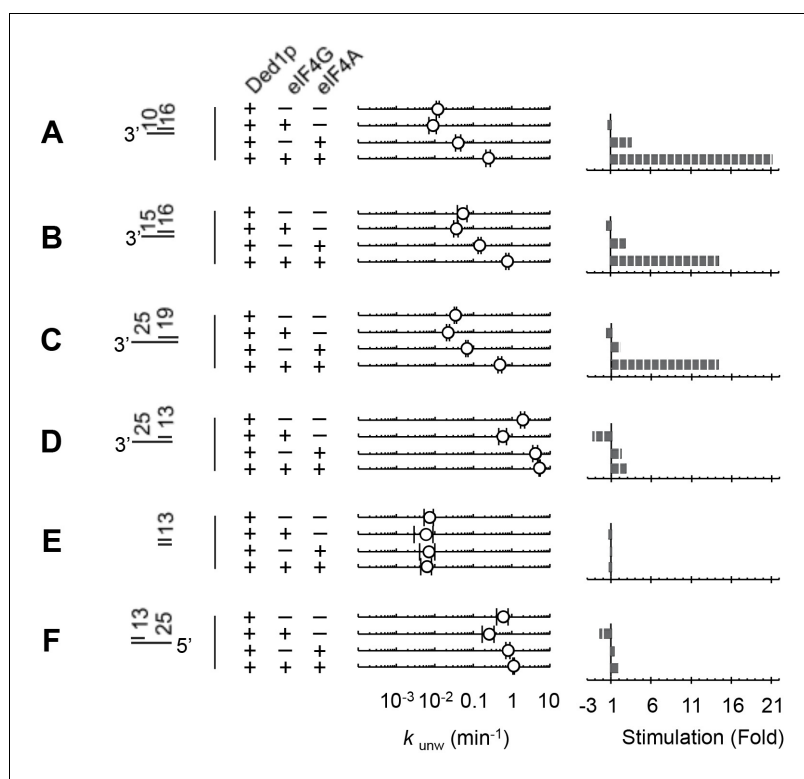


Figure 6—figure supplement 2. Substrate architecture affects the modulation of Ded1p activity by eIF4A and eIF4G. (A–F) Impact of eIF4A, eIF4G, or both on the unwinding activity of Ded1p with different substrates, shown schematically at the left (numbers indicate nucleotides in unpaired overhang and basepairs in duplex region). Reactions were performed as in **Figure 2B**. Sliding point graphs show observed unwinding rate constants (k_{unw} , average of at least three independent measurements), error bars mark one standard deviation. Bar graphs show increase or decrease of k_{unw} compared to the reaction with only Ded1p for each substrate.

DOI: [10.7554/eLife.16408.019](https://doi.org/10.7554/eLife.16408.019)

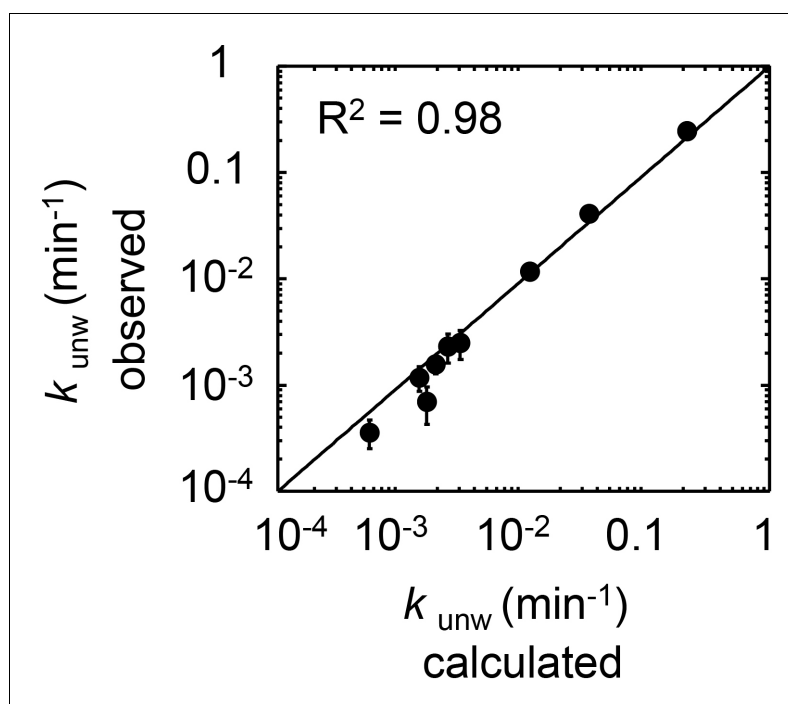


Figure 6—figure supplement 3. Correlation between observed and calculated unwinding rate constants (k_{unw}) for the 16 bp substrate with 10 nt 3' tail. R^2 is the correlation coefficient for the linear fit of the data to a diagonal (black line). Error bars mark the 95% confidence interval for the calculated data.

DOI: [10.7554/eLife.16408.020](https://doi.org/10.7554/eLife.16408.020)

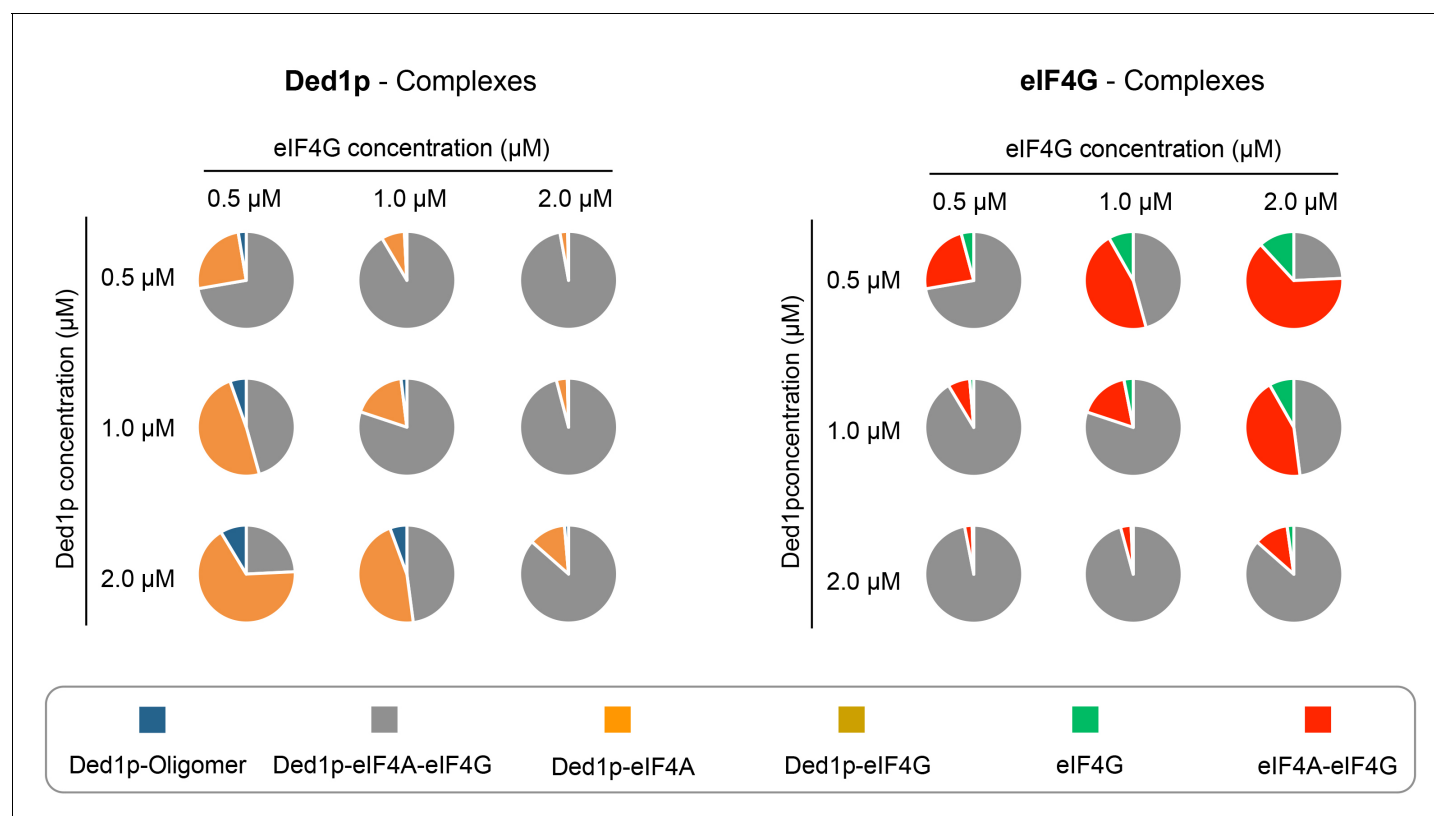


Figure 7. Calculated prevalence of complexes formed between Ded1p, eIF4A and eIF4G at physiological protein concentrations. Fraction of Ded1p (left) and eIF4G (right) present in the various complexes with eIF4A, eIF4G, or both, at three different Ded1p and eIF4G concentrations around their reported physiological concentrations of $\sim 1 \mu\text{M}$ (RNA = $6 \mu\text{M}$, ATP = 2.5 mM). Relative abundance of the complexes were calculated with the binding parameters obtained from the thermodynamic framework (**Figure 4A**, **Supplementary file 2**). See also **Figure 4** and **Supplementary file 2**.

DOI: [10.7554/eLife.16408.021](https://doi.org/10.7554/eLife.16408.021)